Published on 25 June 2015. Downloaded by UNIVERSIDAD ESTADUAL DE CAMPINAS on 03/05/2016 16:53:55.

Nanoscale

ROYAL SOCIETY OF CHEMISTRY

PAPER

View Article Online
View Journal | View Issue

Cite this: *Nanoscale*, 2015, **7**, 12722

Interaction between lamellar twinning and catalyst dynamics in spontaneous core–shell InGaP nanowires†

D. S. Oliveira,*[a] L. H. G. Tizei,[b] A. Li,[c] T. L. Vasconcelos,[d] C. A. Senna,[d] B. S. Archanjo,[d] D. Ugarte[a] and M. A. Cotta[a]

Received 28th April 2015,
Accepted 23rd June 2015

DOI: 10.1039/c5nr02747k

www.rsc.org/nanoscale

Semiconductor nanowires oriented along the [211] direction usually present twins parallel to their axis. For group IV nanowires this kind of twin allows the formation of a catalyst–nanowire interface composed of two equivalent {111} facets. For III–V nanowires, however, the twin will generate two facets with different polarities. In order to keep the <211> orientation stable, a balance in growth rates for these different facets must be reached. We report here the observation of stable, micron-long <211>-oriented InGaP nanowires with a spontaneous core–shell structure. We show that stacking fault formation in the crystal region corresponding to the {111}A facet termination provides a stable NW/NP interface for growth along the <211> direction. During sample cool down, however, the catalyst migrates to a lateral {111}B facet, allowing the growth of branches perpendicular to the initial orientation. In addition to that, we show that the core–shell structure is non-concentric, most likely due to the asymmetry between the facets formed in the NW sidewall; this effect generates stress along the nanowire, which can be relieved through bending.

Introduction

Semiconductor nanowires (NWs) show promising applications for new generations of devices, not only due to their electronic properties but also due to the high degree of control of their synthesis. In particular, the vapor–liquid–solid growth[1–4] method allows a wide variety of materials and structures to be produced with a high degree of control. Indeed, the morphology and crystal structure of semiconductor nanowires can also be used to achieve several interesting attributes, which are not observed in the macroscopic or thin film form of the same substance. For example, GaP nanowires with direct band gaps were obtained when their crystal phase is wurtzite.[5] Also, Si nanowires with rough sidewalls show very low thermal conductivity, what makes them candidates for thermoelectric applications.[6] In contrast, a careful surface passivation of Si nanowires may lead to a significant increase in the field-effect mobility.[7]

For a single material, a reasonably simple way of changing nanowire electronic properties lies in the control of its orientation. Usually, III–V nanowires grow in the [111] direction.[8,9] In this case, nucleation energies for wurtzite (WZ) and zincblend (ZB) monolayers are very similar; therefore, stacking faults are very common. By changing the nanowire orientation to [100][10] or [110][11] growth directions, the nucleation of stacking faults can be avoided. Furthermore, nanowire networks can be implemented by controlling and changing the NW crystallographic axis orientation during growth.[12]

To date, most of the literature on III–V nanowires deals with NW growth along the [111] direction.[4,5,8,13,14] However, a thorough characterization of nanowires grown in different directions is essential to gather a basic understanding of the growth control procedures; it also opens the possibility for new applications. In the case of ternary alloys, the different chemistry at the NP/NW interface may lead to changes in the composition of the semiconductor material, thus allowing a wider range of potential applications, particularly for optical devices.

In this work, we present an extensive study of the structural and morphological properties of core–shell InGaP nanowires. In particular, we have observed very long nanowires of triangular cross section oriented along [211]. These nanowires present interesting characteristics such as a larger In/Ga concentration ratio at the core and the possibility of achieving branched structures in a single growth run.

[a]Instituto de Física "GlebWataghin", Universidade Estadual de Campinas, UNICAMP, 13083-859 Campinas, SP, Brazil. E-mail: doug@ifi.unicamp.br
[b]Laboratoire de Physique des Solides, Université Paris-Sud, CNRS-UMR 8502, Orsay 91405, France
[c]Department of Applied Physics, TU Eindhoven, Den Dolech 2, 5612 AZ Eindhoven, The Netherlands
[d]Divisão de Metrologia de Materiais, Instituto Nacional de Metrologia, Qualidade e Tecnologia (INMETRO), Duque de Caxias, RJ 25250-020, Brazil
† Electronic supplementary information (ESI) available. See DOI: 10.1039/c5nr02747k

This journal is © The Royal Society of Chemistry 2015

Published on 25 June 2015. Downloaded by UNIVERSIDAD ESTADUAL DE CAMPINAS on 03/05/2016 16:53:55.

Methods

Nanowires have been grown in a chemical beam epitaxy (CBE) chamber on GaAs(100) substrates. The substrate native oxide has not been desorbed prior to the growth. Physically deposited gold nanoparticles[15] have been used as catalysts. Tri-ethyl-gallium (TEG) and tri-methyl-indium (TMI) diluted with hydrogen carrier gas and thermally decomposed phosphine (PH_3) have been used as group III and V sources, respectively.

The nanowires were grown at 480 °C using conditions normally used for InGaP thin films lattice-matched to GaAs at higher temperatures.[16] After 45 min, group III precursor flow was turned off, and the sample was cooled down under PH_3 flow (see Fig. S1† for a general overview of the sample).

The samples were firstly observed using scanning electron microscopy (SEM, Inspect F50) for statistical information about nanowire geometry and morphology. Cross-section view samples of the NWs were prepared using dual beam Helios Nanolab 650 and Nova Nanolab 600 microscopes (see Fig. S2† for details). Finally, for the crystalline structure and chemical composition, the samples were analyzed by transmission electron microscopy (TEM) and scanning transmission electron microscopy (STEM); several instruments have been used for the different TEM methods (JEM 3010 URP operated at 300 kV, JEM 2100 ARP and JEM ARM 200F operated at 200 kV, and a probe-corrected FEI Titan operated at 300 kV).

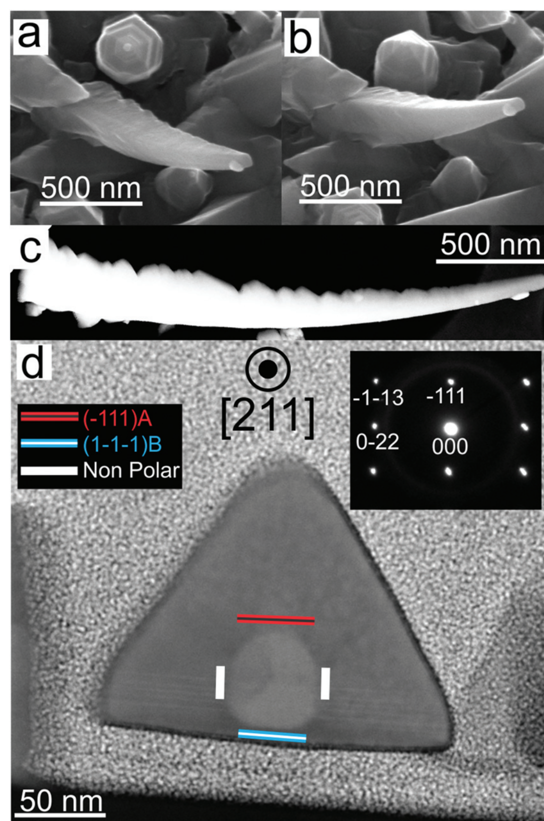

Fig. 1 (a and b) SEM image of as-grown nanowires; the sample was tilted by 30° between images. (c) ADF-STEM lateral view of a triangular NW. (d) TEM image of the cross section of a nanowire grown in the [211] direction (see electron diffraction pattern in the inset).

Results and discussion

Fig. 1a–c show the general morphology of the nanowires. The sample contains mainly (up to ~90%) nanowires with wurtzite atomic structure and hexagonal morphology (see an example in the upper region of Fig. 1a and in Fig. S3;† the metal nanoparticle can be recognized at the nanowire tip). A few of these wurtzite nanowires contain screw dislocations.[17] Also, a second family of nanowires (5–10% of the nanowires) could be found on the substrate, showing several peculiar attributes: (a) triangular cross-section; (b) the nanowires are slightly bent; (c) the catalytic particle is not found at the top of the nanowire; in contrast it is lying on a lateral facet close to the nanowire tip.

In order to obtain deeper structural information on these triangular nanowires we prepared cross sectional TEM samples. TEM images have revealed a core–shell structure with a rather compact core located at a quite eccentric position; in fact the triangular shape of the nanowires is determined by the shell layer which shows quite different thicknesses for different radial directions (see Fig. 1d). Electron diffraction patterns (inset) indicate that these nanowires have a zinc-blende crystallographic structure and their growth axis is parallel to the [211] direction.

For ternary nanowires, the spontaneous formation of a core–shell structure is expected as axial VLS growth is determined by the actual In/Ga supply ratio at the NP/NW interface through the catalyst, which is governed by the solubility of different group III atoms in metal Au nanoparticles.[18,19] Meanwhile, for shell growth, the availability of materials is mostly related with precursor flow and mass transport by surface diffusion. Therefore, the NW shell and core will show different chemical compositions.

This is indeed our case; while the shell is Ga-rich, the core presents a larger In concentration (see Fig. S4 in the ESI† for details).

Core–shell nanowires are usually obtained using a two-step procedure. First, the core is grown through the catalyst by VLS; conditions are subsequently changed to promote preferential vapor–solid growth and the shell is formed. However, if the catalyst is not removed prior to the shell growth, axial growth[20] or kinks in the nanowire[21] are obtained as well. Such effects can be avoided by growing a spontaneous shell. In this case, however, it is more difficult to control thickness variations due to polarity issues.

HRTEM images observed laterally in a [0-11] orientation show that our [211]-oriented, ZB nanowires have *ortho*-twins (LT, lamellar twin) and stacking faults (SF) parallel to the growth direction (Fig. 2a and b). For III–V compounds, an *ortho*-twin will lead to polarity inversion of {111} planes which are not parallel to the twin plane (Fig. S5). Therefore, the <111> sidewalls of the nanowire, which are parallel to the twin

Published on 25 June 2015. Downloaded by UNIVERSIDAD ESTADUAL DE CAMPINAS on 03/05/2016 16:53:55.

plane, will have polarities as shown schematically in Fig. 1d. The non-concentric core–shell structure obtained can be explained by the difference in growth rates for A and B facets,[22] enhanced by strain-related surface diffusion and mass transport.[23] In fact, the non-concentric core–shell morphology is generated on the sidewalls of an In-rich core with larger lattice parameter. Thus, compressive stress develops sooner in the thicker shell region. This stress is eventually relieved through the observed nanowire bending.

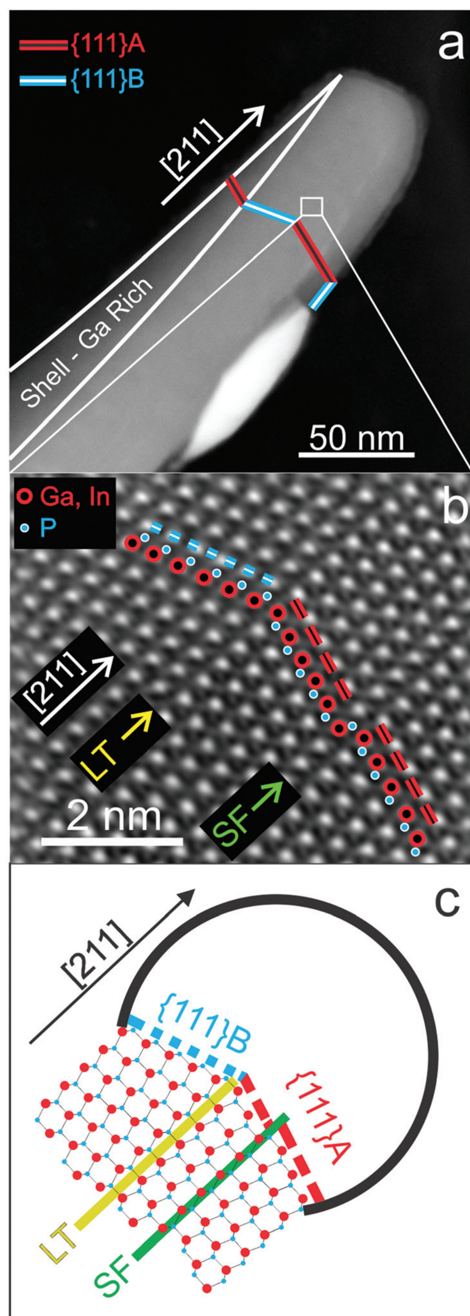

Fig. 2 (a) High angle annular dark field (HAADF) image of a nanowire; the polarity of the {111} facets has been determined by direct measurements of the dumbbells. (b) FFT filtered image of a HAADF image of the region indicated in (a), which shows the presence of LTs and SFs. (c) Schematics of the interface between the catalyst and the nanowire during growth.

For [211]-oriented III–V[24–26] and group IV[27–29] nanowires, lamellar twins are a common feature. For group IV nanowires, twinning allows energy minimization of the nanoparticle–semiconductor interface, which is composed of multiple <111> facets.[29–31] However, for III–V nanowires the nanoparticle–semiconductor interface during axial growth will be composed of facets with different polarities (Fig. 2) which usually present different growth rates.[11,32] In this case, if one side of the LT indeed grows faster than the other, a kink will eventually be formed,[33] since the interface will not remain stable during growth. However, despite these expected instabilities, we could find up to 2 micron long [211]-oriented nanowires (Fig. 1c). In order to keep this growth direction stable, both A and B-terminated interfaces should thus have similar growth rates.

Our nanowires present a small number of LTs. Therefore the catalyst–semiconductor interface is composed of few regions with the same polarity (Fig. 2a and 3); Fig. 3 shows that the number of SFs is much larger on {111}A facets than {111}B.

SFs or twins present at the catalyst–semiconductor interface behave as preferential nucleation sites for VLS growth.[27,29] We can thus expect an enhancement of the {111}A growth rate, as compared to its defect-free counterpart. The presence of SFs can thus balance the growth rates of the different regions composing the catalyst–semiconductor interface, providing stable conditions to the growth of our μm-long, <211>-oriented nanowires.

TEM images show that SFs and LTs are generated during kinking[34] (Fig. S6†), at the sidewall of the nanowire. In fact, it has been demonstrated that the formation of stacking faults[35] and twins[36] is correlated. Therefore, generation of defects during kinking could drive the system towards stable growth in a low probability orientation.

However, it can be expected that at some point the growth gets unstable; in that case, the growth interface most likely changes towards a more energetically favorable direction such as <111>B.[8,37] In our case, this is indeed observed for the nanoparticle final positioning.

A more careful analysis (Fig. 4a) shows that the apex length above the catalyst position is much larger than the shell thickness at similar heights. This is an indication that the catalyst moved to the sidewall of the nanowire after the apex was grown by VLS, according to the schematics in Fig. 4b and c. An interesting example is displayed in Fig. 4a, where we can observe a small gold particle between the nanowire apex and the catalyst nanoparticle. This clearly indicates that catalysts glided down from the apex after the VLS process.

The movement of a nanoparticle towards the nanowire sidewall during growth usually leads to materials deposited along its path.[38] In our case, however, we also observe regions where materials seem to have been removed (Fig. 5a), and defect contrast is discontinued (Fig. 5b). This indicates that NP move-

 This journal is © The Royal Society of Chemistry 2015

Published on 25 June 2015. Downloaded by UNIVERSIDAD ESTADUAL DE CAMPINAS on 03/05/2016 16:53:55.

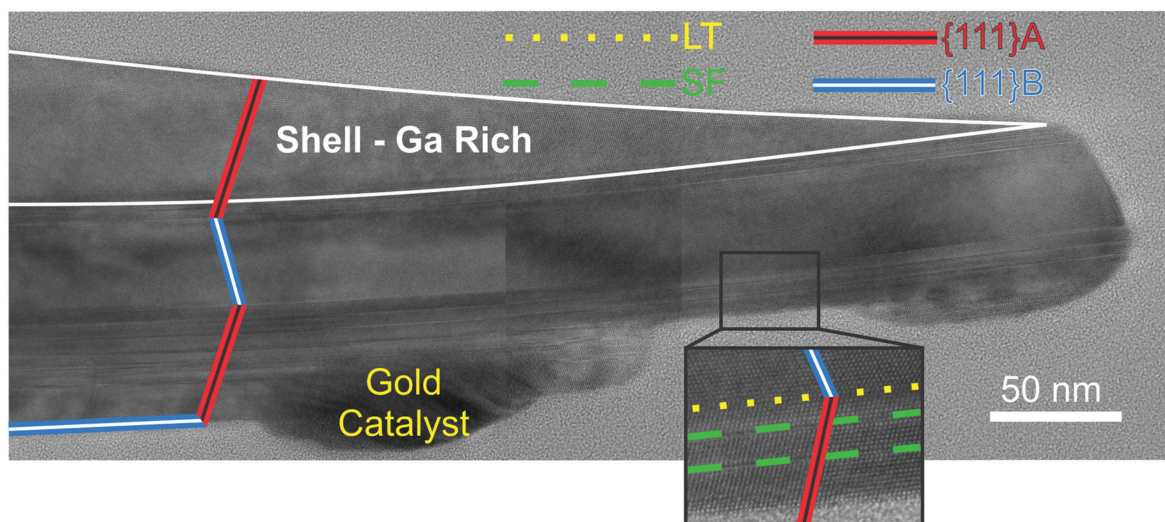

Fig. 3 Mosaic of nanowire HRTEM images. {111} facets with different polarities are enabled by lamellar twins, as indicated in the figure inset. Most of the stacking faults cross the {111}A facet.

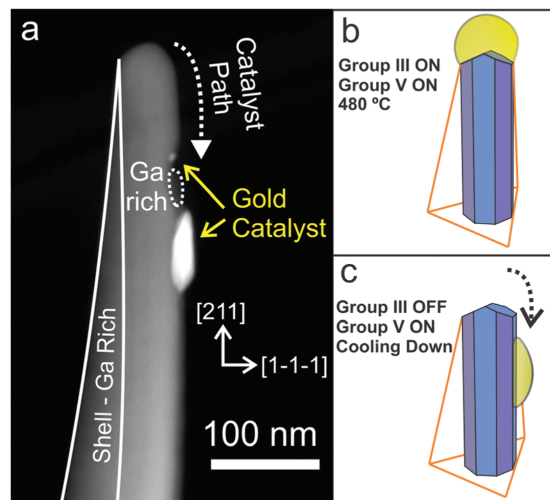

Fig. 4 (a) HAADF image of a nanowire apex. (b) Schematics of the catalyst position during growth. (c) Schematics of the catalyst movement and the final position during cool down.

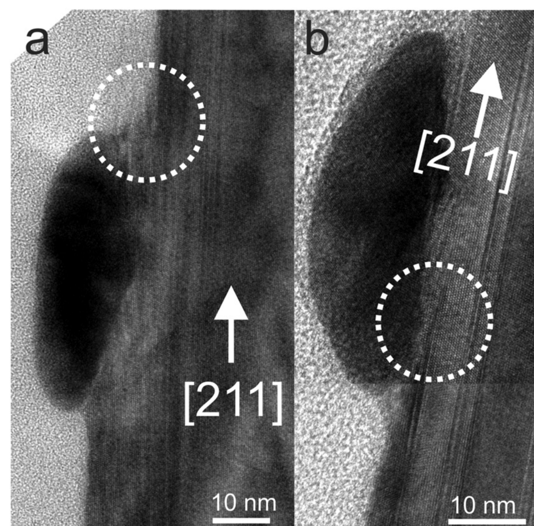

Fig. 5 HRTEM image. (a) The highlights indicate missing regions along the nanowire sidewall. (b) The image shows a discontinued stacking fault, as indicated by the highlights.

ment along the sidewall occurs under a lower saturation environment, with no flow of group III precursors. The final interface between NP and the semiconductor sidewall shows different profiles (Fig. 5a and b), which agrees with a formation process under non-equilibrium conditions during sample cool down, as schematized in Fig. 4b and c. Missing materials along the NP path on the nanowire sidewall can be associated with the reorganization of the underlying surface during catalyst movement.[39]

Nanowire kinking to different directions can be induced by changing the growth conditions (temperature or precursor flow).[40–42] In our case, however, kinking may not occur since group III precursor flow is off during sample cooldown; instead, we observe the catalyst movement to another direction. From the TEM images we could identify that the nanoparticle always moves to the energetically more favorable <111>B direction.[43]

The movement of the NP as a whole indicates that there are net forces acting on it due to chemical potential changes during sample cool down. From Fig. 4, we also identified a Ga-rich region along the nanoparticle path. When In is present, the solubility of Ga on the Au catalyst is reduced.[44] In fact, through EDS measurements we could not identify any Ga in the catalyst after growth (Fig. S7†), or either a clear Ga-rich neck region (Fig. S8†), in case Ga is expelled from the catalyst

Published on 25 June 2015. Downloaded by UNIVERSIDAD ESTADUAL DE CAMPINAS on 03/05/2016 16:53:55.

during sample cool down. The solubility of Ga in the catalyst during growth is thus very small.

Therefore, if the catalyst reorganizes the surface during the movement along the sidewall, it leaves Ga-rich material as a trail due to solubility limitations. The final position of the catalyst must be defined by the latter effect. The volume of shell material (which is Ga-rich) increases for regions closer to the NW bottom; the shell thickness may thus behave like a barrier for the catalyst movement, settling its final position.

The reorganization of the nanowire sidewall due to the catalyst movement allows the formation of a facet that could be used to grow more complex structures; if precursor supply is turned on again after the nanoparticle stops moving along the NW sidewall, a branch can be grown (Fig. S9†). In addition, the final position of the NP can be controlled with the shell thickness. The catalyst would thus be found closer to the apex for more tapered nanowires.

Conclusion

We have grown and characterized [211] InGaP nanowires with a spontaneous core–shell structure. The evolution of shell growth leads to a non-concentric core–shell structure, which, in association with lattice mismatch between the core and the shell, generates stress in the nanowire, relieved through bending.

We also observed that our nanowires present lamellar twinning. LTs allow the formation of more stable facets at the interface between the catalyst and the nanowire. However, for III–V nanowires, LT can also change the interface polarity.

Usually, nanowires with the same orientation and different polarities present different growth rates; this orientation would thus be unstable against kinks, unless the difference in growth rates is balanced. In our micron-long [211]-oriented nanowires, this balance can be achieved through SF formation in the crystal region terminating in a {111}A facet at the NP interface.

Nevertheless, this stability is not very robust, since modifications in the growth conditions can completely change this scenario, as evidenced by the catalyst movement during sample cool down. In this case, the catalyst moves to the {111} B facet, which is perpendicular to the growth direction. This effect can be further explored to obtain full control of complex III–V nanowire network formation.

The observed criteria for stable growth of <211>-oriented III–V nanowires can explain why they are so seldom obtained but are relatively more common to group IV NWs, since LTs in the latter case will not lead to an NW/NP interface with different polarities.

Acknowledgements

We acknowledge the National Laboratory of Nanotechnology (LNNANO/CNPEM) for granting access to their electron microscopy facilities. We also acknowledge Th. Chiaramonte for discussions on NW growth and H. T. Obata for technical assistance. This work was financially supported by FAPESP (grant 2013/02300-1), CNPq (grant 479486/2012-3) and CAPES. D.S. Oliveira acknowledges FAPESP for funding his scholarship.

Notes and references

1 K. Hillerich, K. A. Dick, C.-Y. Wen, M. C. Reuter, S. Kodambaka and F. M. Ross, *Nano Lett.*, 2013, **13**, 903–908.

2 H. J. Joyce, J. Wong-Leung, Q. Gao, H. H. Tan and C. Jagadish, *Nano Lett.*, 2010, **10**, 908–915.

3 Y. Li, F. Qian, J. Xiang and C. Lieber, *Mater. Today*, 2006, **9**, 18–27.

4 R. E. Algra, M. A. Verheijen, M. T. Borgström, L.-F. Feiner, G. Immink, W. J. P. van Enckevort, E. Vlieg and E. P. A. M. Bakkers, *Nature*, 2008, **456**, 369–372.

5 S. Assali, I. Zardo, S. Plissard, D. Kriegner, M. A. Verheijen, G. Bauer, A. Meijerink, A. Belabbes, F. Bechstedt, J. E. M. Haverkort and E. P. A. M. Bakkers, *Nano Lett.*, 2013, **13**, 1559–1563.

6 A. I. Hochbaum, R. Chen, R. D. Delgado, W. Liang, E. C. Garnett, M. Najarian, A. Majumdar and P. Yang, *Nature*, 2008, **451**, 163–167.

7 J. W. W. van Tilburg, R. E. Algra, W. G. G. Immink, M. Verheijen, E. P. A. M. Bakkers and L. P. Kouwenhoven, *Semicond. Sci. Technol.*, 2010, **25**, 024011.

8 J. Johansson, L. S. Karlsson, C. P. T. Svensson, T. Mårtensson, B. A. Wacaser, K. Deppert, L. Samuelson and W. Seifert, *Nat. Mater.*, 2006, **5**, 574–580.

9 S. A. Fortuna and X. Li, *Semicond. Sci. Technol.*, 2010, **25**, 024005.

10 U. Krishnamachari, M. Borgstrom, B. J. Ohlsson, N. Panev, L. Samuelson, W. Seifert, M. W. Larsson and L. R. Wallenberg, *Appl. Phys. Lett.*, 2004, **85**, 2077.

11 Z. H. Wu, X. Mei, D. Kim, M. Blumin, H. E. Ruda, J. Q. Liu and K. L. Kavanagh, *Appl. Phys. Lett.*, 2003, **83**, 3368.

12 D. Car, J. Wang, M. A. Verheijen, E. P. A. M. Bakkers and S. R. Plissard, *Adv. Mater.*, 2014, **26**, 4875–4879.

13 K. A. Dick, K. Deppert, L. Samuelson, L. R. Wallenberg and F. M. Ross, *Nano Lett.*, 2008, **8**, 4087–4091.

14 S. G. Ghalamestani, M. Ek, M. Ghasemi, P. Caroff, J. Johansson and K. A. Dick, *Nanoscale*, 2014, **6**, 1086–1092.

15 K. Kimoto, Y. Kamiya, M. Nonoyama and R. Uyeda, *Jpn. J. Appl. Phys.*, 1963, **2**, 702–713.

16 J. R. R. Bortoleto, H. R. Gutiérrez, M. A. Cotta and J. Bettini, *J. Appl. Phys.*, 2007, 101.

17 L. Tizei, a. Craven, L. Zagonel, M. Tencé, O. Stéphan, T. Chiaramonte, M. Cotta and D. Ugarte, *Phys. Rev. Lett.*, 2011, **107**, 1–5.

18 Y.-N. Guo, H.-Y. Xu, G. J. Auchterlonie, T. Burgess, H. J. Joyce, Q. Gao, H. H. Tan, C. Jagadish, H.-B. Shu, X.-S. Chen, W. Lu, Y. Kim and J. Zou, *Nano Lett.*, 2013, **13**, 643–650.

This journal is © The Royal Society of Chemistry 2015

View Article Online

Published on 25 June 2015. Downloaded by UNIVERSIDAD ESTADUAL DE CAMPINAS on 03/05/2016 16:53:55.

19 A. Fakhr, Y. M. Haddara and R. R. Lapierre, *Nanotechnology*, 2010, **21**, 165601.

20 R. Popovitz-Biro, A. Kretinin, P. Von Huth and H. Shtrikman, *Cryst. Growth Des.*, 2011, **11**, 3858–3865.

21 K. L. Kavanagh, I. Saveliev, M. Blumin, G. Swadener and H. E. Ruda, *J. Appl. Phys.*, 2012, **111**, 044301.

22 T. Burgess, S. Breuer, P. Caroff, J. Wong-Leung, Q. Gao, H. Hoe Tan and C. Jagadish, *ACS Nano*, 2013, **7**, 8105–8114.

23 H. R. Gutiérrez, M. A. Cotta, J. R. R. Bortoleto and M. M. G. de Carvalho, *J. Appl. Phys.*, 2002, **92**, 7523.

24 Z.-A. Li, C. Möller, V. Migunov, M. Spasova, M. Farle, A. Lysov, C. Gutsche, I. Regolin, W. Prost, F.-J. Tegude and P. Ercius, *J. Appl. Phys.*, 2011, **109**, 114320.

25 F. M. Davidson, *J. Phys. Chem. C*, 2007, **111**, 2929–2935.

26 X. Zhang, J. Zou, M. Paladugu, Y. Guo, Y. Wang, Y. Kim, H. J. Joyce, Q. Gao, H. H. Tan and C. Jagadish, *Small*, 2009, **5**, 366–369.

27 S. A. Dayeh, J. Wang, N. Li, J. Y. Huang, A. V. Gin and S. T. Picraux, *Nano Lett.*, 2011, **11**, 4200–4206.

28 N. Shin, M. Chi and M. A. Filler, *ACS Nano*, 2014, **8**, 3829–3835.

29 A. D. Gamalski, P. W. Voorhees, C. Ducati, R. Sharma and S. Hofmann, *Nano Lett.*, 2014, **14**, 1288–1292.

30 C. Cayron, M. Den Hertog, L. Latu-Romain, C. Mouchet, C. Secouard, J.-L. Rouviere, E. Rouviere and J.-P. Simonato, *J. Appl. Crystallogr.*, 2009, **42**, 242–252.

31 A. Stekolnikov and F. Bechstedt, *Phys. Rev. B: Condens. Matter*, 2005, **72**, 125326.

32 B. A. Wacaser, K. Deppert, L. S. Karlsson, L. Samuelson and W. Seifert, *J. Cryst. Growth*, 2006, **287**, 504–508.

33 F. Lenrick, M. Ek, K. Deppert, L. Samuelson and L. R. Wallenberg, *Nano Res.*, 2014, **1**, 1–7.

34 X. Yuan, P. Caroff, J. Wong-Leung, H. H. Tan and C. Jagadish, *Nanoscale*, 2015, **7**, 4995–5003.

35 G. Priante, J.-C. Harmand, G. Patriarche and F. Glas, *Phys. Rev. B: Condens. Matter*, 2014, **89**, 241301.

36 Z. Yuan and A. Nakano, *Nano Lett.*, 2013, **13**, 4925–4930.

37 M. De La Mata, C. Magen, J. Gazquez, M. I. B. Utama, M. Heiss, S. Lopatin, F. Furtmayr, C. J. Fernández-Rojas, B. Peng, J. R. Morante, R. Rurali, M. Eickhoff, A. Fontcuberta I Morral, Q. Xiong and J. Arbiol, *Nano Lett.*, 2012, **12**, 2579–2586.

38 M. Paladugu, J. Zou, Y.-N. Guo, G. J. Auchterlonie, H. J. Joyce, Q. Gao, H. H. Tan, C. Jagadish and Y. Kim, *Small*, 2007, **3**, 1873–1877.

39 J. Wu, Z. M. Wang, A. Z. Li, M. Benamara and G. J. Salamo, *ACS Appl. Mater. Interfaces*, 2011, **3**, 1817–1820.

40 J. Wang, S. Plissard, M. Verheijen, L.-F. Feiner, A. Cavalli and E. P. A. M. Bakkers, *Nano Lett.*, 2013, **13**, 3802–3806.

41 P. Madras, E. Dailey and J. Drucker, *Nano Lett.*, 2009, **9**, 3826–3830.

42 S. Fahlvik Svensson, S. Jeppesen, C. Thelander, L. Samuelson, H. Linke and K. A. Dick, *Nanotechnology*, 2013, **24**, 345601.

43 N. V. Sibirev, M. A. Timofeeva, A. D. Bol'shakov, M. V. Nazarenko and V. G. Dubrovskiĭ, *Phys. Solid State*, 2010, **52**, 1531–1538.

44 M. Paladugu, J. Zou, Y.-N. Guo, X. Zhang, Y. Kim, H. J. Joyce, Q. Gao, H. H. Tan and C. Jagadish, *Appl. Phys. Lett.*, 2008, **93**, 101911.

This journal is © The Royal Society of Chemistry 2015